Publications of the Astronomical Society of the Pacific, 132:064503 (9pp), 2020 June https://doi.org/10.1088/1538-3873/ab7d1d

Estimating Statistical Uncertainties of Internal Kinematics of Galaxies and Star Clusters Derived Using Full Spectrum Fitting*

Igor V. Chilingarian[1,2] and Kirill A. Grishin[2,3]
[1] Smithsonian Astrophysical Observatory, 60 Garden St. MS09, Cambridge, MA 02138, USA; igor.chilingarian@cfa.harvard.edu, chil@sai.msu.ru
[2] Sternberg Astronomical Institute, M.V. Lomonosov Moscow State University, Universitetsky prospect 13, Moscow, 119234, Russia
[3] Department of Physics, M.V. Lomonosov Moscow State University, 1 Vorobyovy Gory, Moscow, 119991, Russia
Received 2019 December 11; accepted 2020 March 5; published 2020 April 21

Abstract

Pixel-space full spectrum fitting exploiting nonlinear χ^2 minimization became a *de facto* standard way of deriving internal kinematics from absorption line spectra of galaxies and star clusters. However, reliable estimation of uncertainties for kinematic parameters remains a challenge and is usually addressed by running computationally expensive Monte-Carlo simulations. Here we derive simple formulae for the radial velocity and velocity dispersion uncertainties based solely on the shape of a template spectrum used in the fitting procedure and signal-to-noise information. Comparison with Monte-Carlo simulations provides agreement within a few per cent for different templates, signal-to-noise ratios and input velocity dispersions between 0.5 and 10 times the instrumental spectral resolution. For moderate template mismatch our technique returns uncertainties consistent within 20%–30% with those reported by Monte-Carlo simulations. We provide IDL and PYTHON implementations of our approach. The main applications are: (i) exposure time calculators; (ii) design of observational programs and estimates on expected uncertainties for spectral surveys of galaxies and star clusters; (iii) a cheap and accurate substitute for Monte-Carlo simulations when running them for large samples of thousands of spectra is unfeasible.

Unified Astronomy Thesaurus concepts: Analytical mathematics (38); Astronomy data analysis (1858); Galaxy kinematics (602); Galaxy dynamics (591)

Online material: color figures

1. Introduction and Motivation

Stellar and gas kinematics in galaxies keeps a fossil record of their evolution. By analyzing the motions of stars and comparing them to dynamical models, we can derive important properties of a stellar system such as its total mass, a density profile, a degree of rotational support (see e.g., Cappellari 2008). By comparing observations against stellar population models, we can also get an insight on the stellar content of a galaxy or a star cluster. All this information can be extracted from spectra integrated along the line of sight. A pixel-space fitting approach, when a galaxy spectrum is approximated by a template and analyzed in every pixel along the wavelength axis was initially proposed by Rix & White (1992) and then slightly modified and greatly popularized by Cappellari & Emsellem (2004), Cappellari (2017). Their "penalized pixel-fitting" or PPXF technique based on a constrained nonlinear χ^2 minimization became a *de facto* standard way of extracting kinematics from absorption line spectra.

An important aspect of data analysis is the estimation of systematic and statistical uncertainties of parameters returned by a data analysis technique, because they can potentially render an obtained result statistically insignificant. Systematic errors, which might originate from an incomplete knowledge of how a data set was obtained or from degeneracy between parameters of a model, can be very hard to assess. But even statistical uncertainties can be difficult to estimate, especially when a data analysis technique is complex. A typical approach is to use Monte-Carlo simulations to obtain statistical errors by directly analyzing a distribution of solutions from different noise realizations. Despite the simplicity of this approach, it is computationally intensive and the time required to properly sample a multi-dimensional parameter space skyrockets with the increasing number of dimensions.

Monte-Carlo simulations are recommended as a preferred method for estimating the uncertainties of galaxy kinematics in the PPXF documentation, because the formal uncertainties returned by a constrained nonlinear minimization procedure can sometimes be unreliable, e.g., when parameters are degenerated or some of them reach a limit set by a constraint (see e.g., Westfall et al. 2019). However, this can become prohibitively expensive when dealing with large samples of spectra. When we were preparing the Reference Catalog of Spectral Energy Distribution (Chilingarian et al. 2017), we

* The source code is available in a public GIT repository under the GPLv3 license: https://bitbucket.org/extragalactic/pxf_kin_err.

re-fitted a sample of about 800,000 spectra multiple times varying different parameters of the fitting procedure and each step took over a day on a small computer cluster with a single call of the NBURSTS code (Chilingarian et al. 2007a, 2007b), which was derived from PPXF and expanded to fit parametric star formation histories and multiple kinematic components. Running even 1000 Monte-Carlo realizations for every spectrum would have turned it into months so that the project would be never finished.

The motivation of this work has two main aspects. On one hand, it is important to have a reliable approach to quickly estimate uncertainties for galaxy kinematics for a large number of spectra produced by spectroscopic surveys. On the other hand, it is often useful to predict the accuracy of kinematics extracted from a spectrum that has been published but has not been made available in a numerical form or has not yet been collected, e.g., while developing strategies for observational campaigns, preparing new observations, writing telescope time proposals, etc. In other words, one needs a simple formula, which can be plugged into a telescope exposure time calculator assuming that a full spectrum fitting technique will be used to extract galaxy kinematics from a spectrum.

We derive the following formulae for uncertainties of v and σ obtained in the full spectrum fitting with a purely Gaussian LOSVD $\mathcal{L}(v, \sigma)$

$$\begin{aligned}
&\Delta v = \sigma / \sqrt{\textstyle\sum_{N_\lambda} (T * (\mathcal{L}H_1))_i^2 \, \mathrm{SNR}_i^2}; \\
&\Delta \sigma = \sigma / \sqrt{\textstyle\sum_{N_\lambda} (T * (\mathcal{L}H_2))_i^2 \, \mathrm{SNR}_i^2} \\
&\text{where } H_1 = x/\sigma;\ H_2 = x^2/\sigma^2 - 1; \\
&\mathcal{L}(v, \sigma) = \frac{1}{\sigma\sqrt{2\pi}} \exp\left(-\frac{(x-v)^2}{2\sigma^2}\right)
\end{aligned} \tag{1}$$

for a template T spectrum convolved with an instrumental line-spread function of a spectrograph and normalized to its own mean value (mean(T) = 1). Here "$*$" denotes a convolution, σ is a velocity dispersion value, and the sums are done over all pixels. In a simplified case of constant flux uncertainties corresponding to some mean signal-to-noise ratio in a spectrum, the formulae become:

$$\begin{aligned}
\Delta v &= \frac{\sigma}{\mathrm{SNR}} \Big/ \sqrt{\textstyle\sum_{N_\lambda} (T * (\mathcal{L}H_1))_i^2}; \\
\Delta \sigma &= \frac{\sigma}{\mathrm{SNR}} \Big/ \sqrt{\textstyle\sum_{N_\lambda} (T * (\mathcal{L}H_2))_i^2}.
\end{aligned} \tag{2}$$

2. Derivation of the Formulae for v and σ Uncertainties

A pixel space fitting problem using a linear combination of several template spectra can be formulated as a minimization of the following functional (Cappellari & Emsellem 2004; Chilingarian et al. 2007b; Cappellari 2017):

$$\begin{aligned}
&\chi^2 = \textstyle\sum_{N_\lambda} \dfrac{[F_i - P_{1p}\{(\mathcal{T} * \mathcal{L}(v, \sigma, h_3, h_4))_i + P_{2q}\}]^2}{\Delta F_i^2}, \\
&\text{where} \quad \mathcal{T}_i = \textstyle\sum_{N_{\mathrm{mod}}} k_m M_i.
\end{aligned} \tag{3}$$

Here $\mathcal{L}$ is the line-of-sight velocity distribution in the Gauss–Hermite parameterization (van der Marel & Franx 1993); F_i and ΔF_i are observed flux and its uncertainty; $\mathcal{T}_i$ is the flux from a synthetic spectrum, represented by a linear combination of N_{mod} templates M_i and convolved according to the line-spread function of the spectrograph; P_{1p} and P_{2q} are multiplicative and additive Legendre polynomials of orders p and q for correcting the spectral continuum. For the subsequent calculation we consider that the weights k_m are known and fixed, i.e., we deal with a single template $\mathcal{T}_i$. We include multiplicative continuum terms, which match the $\mathcal{T}_i$ and F_i flux scales into that template. Hereafter we denote $\mathcal{T}$ with the included multiplicative continuum as T. We consider a pure Gaussian LOSVD and note that a full Gauss–Hermite LOSVD representation can also be used but the calculations become bulky and one also has to keep in mind the correlations of v with $h3$ and σ with $-h4$. We do not include additive continuum terms. Hence, the expression for χ^2 is simplified:

$$\chi^2(v, \sigma) = \sum_{N_\lambda} \frac{(F_i - (T * \mathcal{L}(v, \sigma))_i)^2}{\Delta F_i^2}. \tag{4}$$

Throughout the calculations we assume that (i) χ^2 changes slowly and monotonically on both sides of the minimum on every parameter; (ii) the parameters are not correlated, which is true for v and σ (Rix & White 1992); (iii) the number of samples in a spectrum is large enough so that the conversion from discrete to continuous formulation does not change the calculation; (iv) there is no template mismatch, that is a real spectrum is well represented by a template and the flux errors in a real spectrum are Gaussian and correctly estimated so that the normalized by degrees of freedom $\chi^2/\mathrm{dof} = 1$.

A minimum of χ^2 is reached at the point (v_0, σ_0) where partial derivatives turn to zero:

$$\left.\frac{\partial \chi^2}{\partial v}\right|_{v_0} = 0; \quad \left.\frac{\partial \chi^2}{\partial \sigma}\right|_{\sigma_0} = 0. \tag{5}$$

To estimate the uncertainties of v and σ we use a standard approach from calculus, a Taylor series expansion of χ^2 at (v_0, σ_0) to the second degree term and finding a value of a parameter p near the minimum where $\chi^2 = \chi^2_{\mathrm{min}} + 1$ (see e.g.,

Sections 15.5 and 15.6.5 in Press et al. 2007):

$$\chi^2(p_0 + \Delta p) = \chi^2(p_0) + 1,$$
$$\frac{\Delta p^2}{2}\frac{\partial^2\chi^2}{\partial p^2}\Bigg|_{p_0} = 1,$$
$$\Delta p = \sqrt{2}/\sqrt{\frac{\partial^2\chi^2}{\partial p^2}\Big|_{p_0}}. \quad (6)$$

Because here we treat each parameter independently, we use the $\Delta\chi^2 = 1$ to estimate the uncertainties rather than higher values suggested by the Pearson χ^2 statistics for multiple parameters (e.g., 2.3 for two and 3.5 for three variables, see Table 1 in Avni 1976).

The second partial derivative of χ^2 from Equation (4) at (v_0, σ_0) are expressed as:

$$\frac{\partial^2\chi^2}{\partial p^2}\Bigg|_{p_0} = \left\{2\left(\sum\left[\left(\frac{\partial}{\partial p}(T * \mathcal{L})_i\right)^2/\Delta F_i^2\right]\right) - 2\sum\left[(F_i - (T * \mathcal{L})_i)\frac{\partial^2}{\partial p^2}(T * \mathcal{L})_i/\Delta F_i^2\right]\right\}\Bigg|_{p_0}. \quad (7)$$

If there is no template mismatch, then at the minimum of χ^2 the second sum becomes zero, because at every pixel in a spectrum the term $(F_i - (T * \mathcal{L})_i)$ is a normally distributed random number with a mathematical expectation of zero. Therefore, we need to compute only first derivatives of a convolution of a template with a LOSVD, and the final result will not depend on the shape of an observed spectrum F_i but rather on a template used to fit it (prior to the convolution with a LOSVD) and flux uncertainties ΔF_i. Then the final formula for the uncertainties becomes:

$$\Delta p = \sqrt{2}/\sqrt{\sum\left[\left(\frac{\partial}{\partial p}(T * \mathcal{L})_i\right)^2/\Delta F_i^2\right]\Big|_{p_0}}. \quad (8)$$

Now we can write an integral form of a convolution going from a discrete to continuous formulation (T_i to $T(\lambda)$) and then compute a derivative directly. After trivial calculations, we obtain:

$$\frac{\partial}{\partial v}(T(\lambda) * \mathcal{L}) = \frac{1}{\sigma^2\sqrt{2\pi}}\int_{-\infty}^{\infty} T(\lambda - x)\frac{(x - v)}{\sigma} \times \exp\left(-\frac{(x - v)^2}{2\sigma^2}\right)dx = \frac{1}{\sigma}\int_{-\infty}^{\infty} T(\lambda - x)\frac{(x - v)}{\sigma}\mathcal{L}(v, \sigma)dx$$

$$\frac{\partial}{\partial \sigma}(T(\lambda) * \mathcal{L}) = \frac{1}{\sigma^2\sqrt{2\pi}}\int_{-\infty}^{\infty} T(\lambda - x)\left(\frac{(x - v)^2}{\sigma^2} - 1\right) \times \exp\left(-\frac{(x - v)^2}{2\sigma^2}\right)dx = \frac{1}{\sigma}\int_{-\infty}^{\infty} T(\lambda - x)\left(\frac{(x - v)^2}{\sigma^2} - 1\right)\mathcal{L}(v, \sigma)dx. \quad (9)$$

We note that each integral in Equation (9) also represents a convolution. In case of Δv the kernel is a Gaussian multiplied by the 1st order Hermite polynomial $H_1 = x/\sigma$ and in case of $\Delta\sigma$ it is a Gaussian multiplied by the 2nd order Hermite polynomial $H_2 = (x/\sigma)^2 - 1$. Now by combining Equations (9) and (8) and substituting ΔF_i with $1/\mathrm{SNR}_i$ under assumptions that the flux scales of T and F_i match and there is no template mismatch, we obtain Equations (1) and (2).

We can also explore a situation when template mismatch presents. Then mathematical expectation of $F_i - (T * \mathcal{L})_i$ in the second term in Equation (7) will not be zero and the term will not automatically zero out because of this. However, as long as the LOSVD is a Gaussian, its derivative, so as the derivative of a convolution integral are expressed as a product of $\mathcal{L}$ and a linear combination of low-order Hermite polynomials. For example, $\frac{\partial^2}{\partial\sigma^2}(T * \mathcal{L})_i$ includes only the Hermite polynomials of orders 2 and 4 and for $\frac{\partial^2}{\partial v^2}(T * \mathcal{L})_i$ the Hermite polynomial order will be 2. Then, if we expand the template mismatch expression $F_i - (T * \mathcal{L})_i$ on the Hermite polynomials basis keeping in mind that they are orthogonal with the weights $\exp(-x^2)$, which is exactly $\mathcal{L}^2$, and replace the sum with an integral, then the only non-zero terms will be those corresponding to low-order Hermite polynomials ($n \leqslant 4$). They correspond to a large-scale template mismatch, which is expected to be compensated by multiplicative continuum terms when running PPXF. Small-scale template mismatch, i.e., absorption line depth difference represented by very high-order polynomials in the Hermite expansion, will not contribute to the second sum in Equation (7). Hence, even when template mismatch presents, with a proper choice of the multiplicative continuum degree (*mdegree*), the second sum in Equation (7) will also turn to zero, and the expression for the uncertainty Equation (8) will stay valid, even though because the template T_i does not well represent the real spectrum, the resulting estimates of uncertainties might get biased.

3. Implementation and Code Availability

We implemented the algorithm described above in a form of code in IDL and PYTHON. Both implementations yield identical results provided the same input data.

The code implements two different approaches for convolution, a direct pixel-space convolution and a convolution in the Fourier space (default option for the code), which correctly handles undersampled kernels in case of small velocity dispersion values of an order of 1 pix and below (see discussion in Cappellari 2017). The input parameters for the function ESTIMATE_PXF_KIN_ERR are: a one-dimensional array of wavelengths, a template spectrum, a value of velocity dispersion, signal-to-noise ratio either per pixel (Equation (1)) or a mean value for the whole spectrum (Equation (2)) and a keyword to choose a convolution technique. If a signal-to-noise array (i.e., $F_i/\Delta F_i$) is correctly computed by a data reduction pipeline, then the quality of flux calibration of an observed spectrum will not affect at all the final result.

The IDL version of the code does not require any third-party dependencies and can be run under IDL version >4.0 or GNU Data Language GDL version >1.0.

The PYTHON version of the code works for both PYTHON 2.7 and PYTHON 3 and requires only a standard NUMPY library (version >1.15.0).

4. Tests Using Monte-Carlo Simulations with Mock Data

We ran a suite of Monte-Carlo simulations using mock data to validate Equation (1) and demonstrate the consistency between uncertainties predicted by the formulae and "real" values computed directly from running a pixel-space fitting code.

We took 9 simple stellar population templates computed with the PEGASE.HR code (Le Borgne et al. 2004) at a spectral resolution $R = 10{,}000$ for three different ages, 200 Myr (young), 2000 Myr (intermediate-age), and 10 Gyr (old), and three metallicities [Fe/H] $= -1.0, -0.5, 0.0$ dex. The average depth of absorption lines in galaxy spectra in the optical wavelength range grows when increasing the age and metallicity and the chosen values of stellar population parameters cover a vast majority of cases one has to deal with in real galaxies and star clusters.

We convolved the original templates to a spectral resolution of 25 km s^{-1}, re-binned them to a scale of 20 km s^{-1} per pixel, and restricted the wavelength range to $3900 < \lambda < 5300$ Å, which roughly correspond to the 1000 gpm intermediate-resolution spectral mode of the Binospec spectrograph (Fabricant et al. 2019), which we used on several occasions to study internal kinematics and stellar populations of galaxies and star clusters. We chose 7 values of expected velocity dispersion from 20 to 300 km s^{-1} and 6 values of signal-to-noise ratio between 3 and 100 per pixel.

We ran the IDL implementation of the PPXF code version 5.2.4 (released on 2018 March 2) for 1000 noise realizations for every set of parameters (age, metallicity, σ, SNR), a total of 378,000 simulations, using no additive continuum (*degree* $= -1$) and the 3rd order multiplicative continuum (*mdegree* $= 3$). We used a corresponding model prior to convolution with the LOSVD as a template to avoid template mismatch by construction. We defined a noise vector for every spectrum as a set of normally distributed random numbers with the dispersion F_i/SNR in the ith pixel. Then we computed uncertainties of v and σ for every numerical experiment as a standard deviation of v and σ reported by PPXF from 1000 realizations. In the end, we compare the uncertainties predicted by Equation (1) to the results of simulations.

The results of simulations are presented in Figure 1. The top set of panels shows estimated uncertainties of v and the bottom panels are for σ. For every age and metallicity there are two panels, which show values of uncertainties (top) and ratios between predicted and computed uncertainties (bottom). The colored lines correspond to different values of the input signal-to-noise ratio.

We see excellent agreement within a few per cent between the uncertainties predicted by our approach and derived from Monte-Carlo simulations. One should keep in mind that 1000 realizations yield an internal statistical accuracy of uncertainties of 1.6%. In a few cases, especially for Δv we see a slight trend toward high velocity dispersion where Equation (1) seem to under-predict the uncertainties by up-to 10%. This, however, might be the result of a worse convergence of the nonlinear minimization used in PPXF, which lead to a higher spread of solutions. We attribute a larger disagreement for low-SNR simulations (3 and 5) to the same effect.

In Figure 1 we also compare our predictions of uncertainties with those computed using Hessian matrices (see e.g., Press et al. 2007) and returned by the Levenberg–Marquadt minimization used by the PPXF code. The ratios of uncertainties are shown by solid black lines in a lower panel for every template. The black lines lay almost exactly on top of each other for every signal-to-noise ratio, trace fairly well the overall behavior of Monte-Carlo simulations, and exhibit similar trends at high input velocity dispersions.

In many cases, the PPXF code is used with a linear combination of templates (rather than with a single template, which is often the case for NBURSTS), whose weights are fitted in a separate constrained linear minimization loop at every evaluation of the functional within the nonlinear fitting. To demonstrate the effect of including several templates in a fitting procedure, we ran 1000 Monte-Carlo realizations for one of the stellar population models (age: 2000 Myr, metallicity: -0.5 dex), which we fitted with a linear combination of all 9 stellar population templates described above. We applied our formula for uncertainties to the resulting linear combination of templates returned by PPXF, which is of course an artificial situation, because these weights are not known a priori. In Figure 2 we present the result of these simulations. The overall behavior of radial velocity uncertainties remains identical to the single template case, however for velocity dispersions both the uncertainties returned by the minimization procedure and those directly computed from the Monte-Carlo

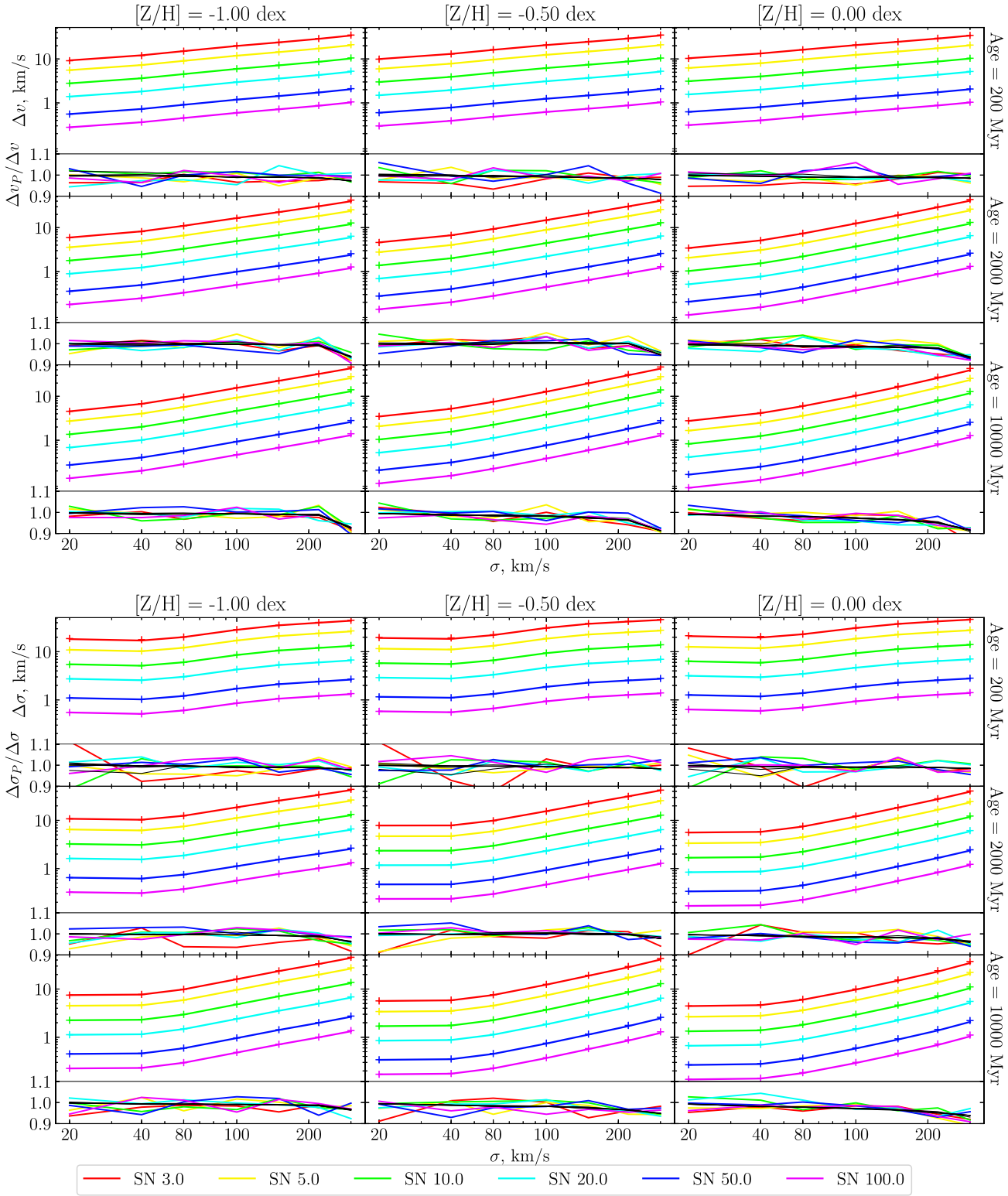

Figure 1. Dependence of the v (top set of panels) and σ uncertainties (bottom set of panel) on the velocity dispersion for 9 templates corresponding to different ages and metallicities. Trends for different signal-to-noise ratios as functions of input σ are shown using different colors. Plus symbols represent the results of Monte-Carlo simulations with 1000 realizations, and lines are predictions using Equation (1). Narrow panels present a ratio of estimated uncertainties to the results of Monte-Carlo simulations.

(A color version of this figure is available in the online journal.)

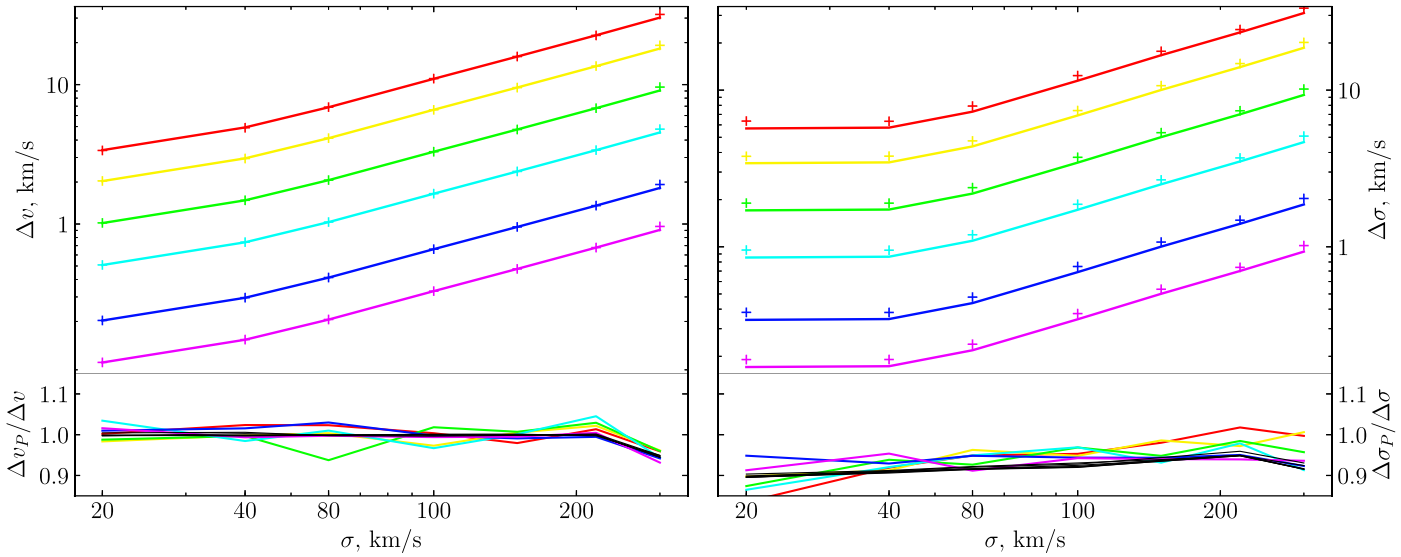

Figure 2. Results of Monte-Carlo simulations (v on the left and σ on the right) for a stellar population model having age 2000 Myr and metallicity −0.5 dex fitted with a linear combination of all 9 templates presented in Figure 1. All labels and notations are the same as in Figure 1.
(A color version of this figure is available in the online journal.)

realizations are higher than those predicted by our approach by some 8%–10%.

We also ran three sets of Monte-Carlo simulations to study the effect of template mismatch. We fitted a model (age: 2000 Myr, metallicity: −0.5 dex) with a template spectrum having older age (10,000 Myr) and the same metallicity and higher metallicity (+0.0 dex) for the same age (Figure 3, upper panels)—these two cases represent a situation when an observed spectrum has shallower absorption lines than a template used to analyze it. The results are qualitatively similar, therefore we present only the case with a metallicity mismatch. Then we ran another series of 1000 realizations but this time using a metal-poor template (−1.0 dex) of the same age (2000 Myr) to model a situation when an observed spectrum has deeper absorption lines compared to a template (Figure 3, lower panels). We also increased the degree of the multiplicative polynomial continuum from 3 to 15 to better compensate for the difference in the continuum shape between the templates.

The estimated uncertainties of both velocities and velocity dispersions suffer biases with the opposite trends when comparing the cases of deeper and shallower absorption lines. The bias does not depend on the signal-to-noise ratio and is defined solely by the template mismatch. The velocity uncertainties predicted by our approach are systematically lower at small input velocity dispersions for a template with deeper absorption lines (higher metallicity) than an observed spectrum and higher for a template with shallower lines (lower metallicity). At high input velocity dispersions, the difference between predicted and computed velocity uncertainties decreases because of the smoothing effect of a broad LOSVD that erases small spectral features. The behavior of velocity dispersion uncertainties is more complex than a simple monotonic trend. In particular, the Hessian matrix based error estimates differ from those estimated from Monte-Carlo simulations. The pattern of bias for uncertainty estimates has a minimum at $\sigma_{\rm input} = 80$–$100\,{\rm km\,s^{-1}}$, that corresponds to 3–4 pix for a higher metallicity template and a maximum for a lower metallicity template; the behavior of the bias as a function of $\sigma_{\rm input}$ is opposite for the two cases, similarly to the radial velocity uncertainties. We notice that we could not measure velocity dispersion using a metal-poor template at $\sigma_{\rm input}$ because the best-fitting values reported by PPXF were below the instrumental resolution of $25\,{\rm km\,s^{-1}}$ because of the metallicity—velocity dispersion degeneracy (Chilingarian 2006; Chilingarian et al. 2007b). Overall, the uncertainties predicted by our technique remain within 20%–30% of those computed using Monte-Carlo simulations in case of moderate template mismatch.

5. Discussion

5.1. Dependence of Uncertainties on a Shape of a Spectrum

The computation of uncertainties presented in Equation (1) has some interesting properties.

1. Uncertainties on both parameters increase when σ grows, which is easy to explain: higher velocity dispersion smooths a spectrum making both v and σ more uncertain.

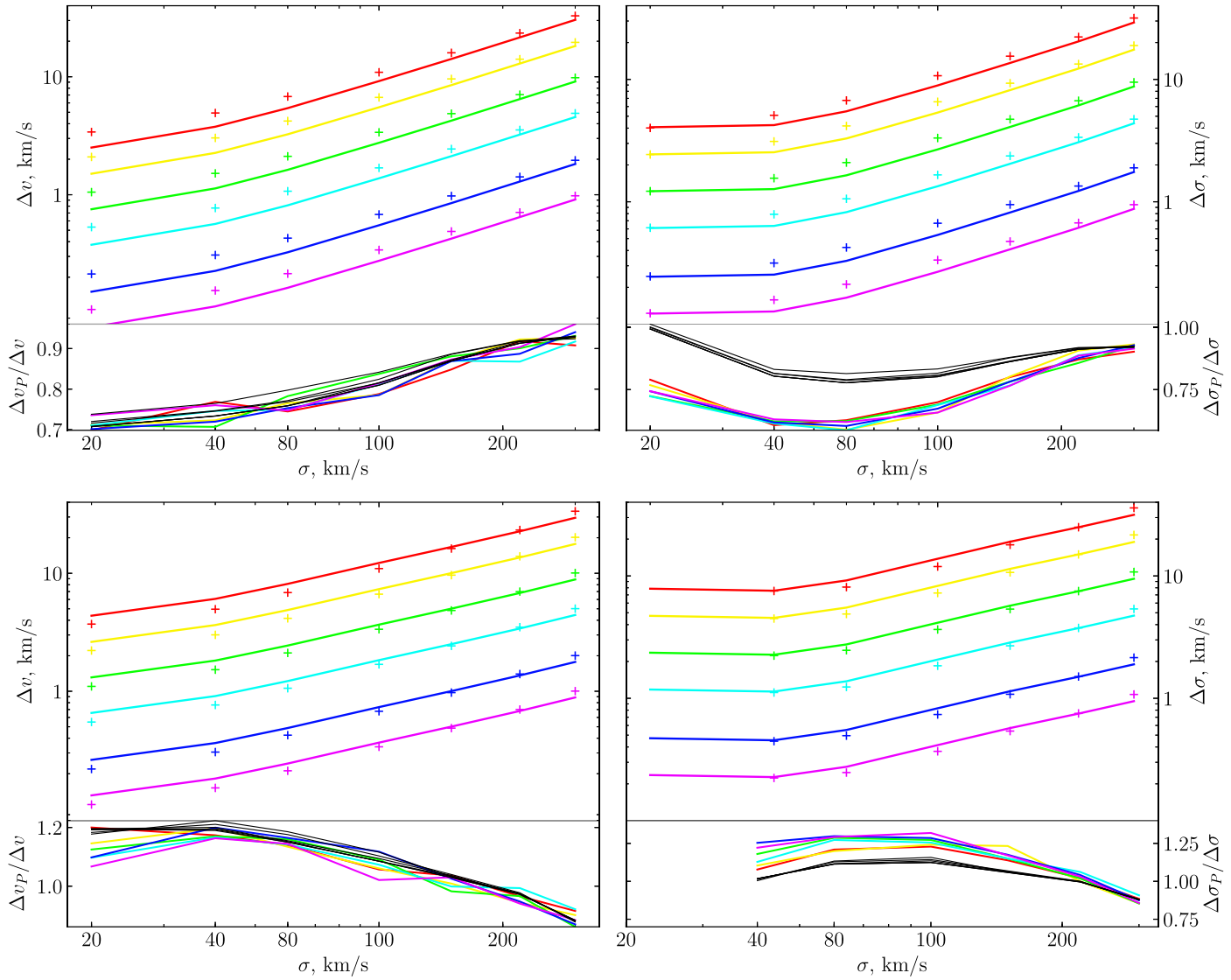

Figure 3. Effects of template mismatch (metallicity): a model having age 2000 Myr and metallicity −0.5 dex is fitted with a template having age 2000 Myr and metallicity +0.0 dex (upper panels) and −1.0 dex (lower panels). All labels and notations are the same as in Figure 1.
(A color version of this figure is available in the online journal.)

2. The convolution kernels $\mathcal{L}H_1$ and $\mathcal{L}H_2$ both have zero total values, therefore a sum of all pixels in a template spectrum convolved with them will be close to zero. However, because the convolution result is squared, the sum will always be positive.
3. The convolution $(T_i * (\mathcal{L}H_1))$ is in fact a two-sided first numerical derivative of a template T_i in terms of finite differences convolved with a Gaussian $\mathcal{L}$ (see Figure 4 left). The convolution and numerical derivation can be done in any order because it is equivalent to a double convolution with the (−0.5, 0, +0.5) kernel and a Gaussian; and a convolution is commutative. Therefore, a local gradient of a convolved template spectrum determines the quality of radial velocity determination: deep broad and narrow spectral lines and sharp continuum breaks both improve the quality.
4. The convolution $(T_i * (\mathcal{L}H_2))$ is a second derivative of T_i in terms of finite differences expressed as a convolution of a template with the (+0.5, −1, +0.5) kernel then convolved with a Gaussian $\mathcal{L}$ (see Figure 4 right). Therefore, a local curvature of a convolved template spectrum determines the quality of velocity dispersion measurements: deep narrow spectral lines are crucial, while broad lines and continuum breaks do not improve the quality.

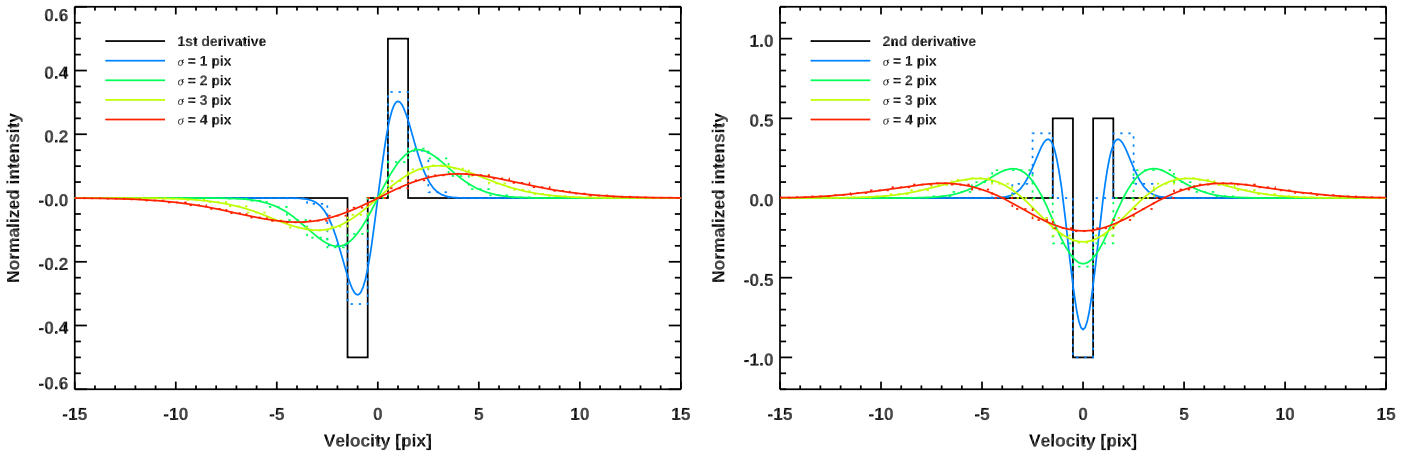

Figure 4. Convolution kernels for the calculation of uncertainties of radial velocity (left) and velocity dispersion (right). Black solid histograms show convolution kernels for the computation of the 1st (left) and 2nd (right) derivatives using finite differences. Colored lines show the convolution kernels $H_1\mathcal{L}$ (left) and $H_2\mathcal{L}$ (right) for several values of the velocity dispersion (see insets for details). Colored dotted histograms show the discrete representation of the corresponding convolution kernels.

(A color version of this figure is available in the online journal.)

One can see a few notable trends in Figure 1.

1. In the chosen wavelength range, which is quite common for extragalactic observations, the uncertainties of v and σ are similar in absolute values when $\sigma > \sigma_{\rm LSF}$.
2. The instrumental resolution (25 km s^{-1}) puts an effective lower limit on the measurement of σ (see the curves flatten at lower σ values below the instrumental resolution). This is trivially explained when one keeps in mind that the instrumental resolution is a convolution of a "true" template spectrum with a line-spread-function (Gaussian in our case). Using the commutativity of the convolution and the property of a Gaussian dispersion during convolution ($\sigma^2_{\rm conv} = \sigma^2_{\rm orig} + \sigma^2_{\rm kernel}$), we conclude that this behavior of uncertainties is an effect of simple error propagation, because the spectrum fitting effectively measures $\sigma^2_{\rm galaxy} + \sigma^2_{\rm LSF}$.
3. However, the flattening is much less pronounced for radial velocities, which one would expect from the fact that Δv depends on a local gradient of the spectral shape, which is less affected by smoothing than a local curvature, that $\Delta\sigma$ depends on.
4. The absolute values of uncertainties grow toward younger ages and lower metallicities, which illustrates the fact that absorption features become less pronounced.
5. The uncertainties are inversely proportional to the signal-to-noise ratio even in very noisy spectra at SNR $= 3-5$.

5.2. Real Data Examples and Potential Caveats

We started the development of our approach while analyzing low signal-to-noise spectral data collected with Binospec at the 6.5 m converted Multiple Mirror Telescope for low surface brightness galaxies in the Coma cluster published in Chilingarian et al. (2019). Our velocity dispersion estimates from intermediate-resolution ($R \approx 4800$) spectra having low signal-to-noise ratio of 4–5 per pixel were questioned by colleagues, in particular by comparing our σ uncertainties (7–9 km s^{-1}) to those (7 km s^{-1}) obtained by van Dokkum et al. (2016) for a similar ultra-diffuse galaxy DF 44 using a larger 10 m Keck telescope and much longer integration time (33.5 hr versus 2 hr) that yielded a substantially higher signal-to-noise ratio of 14 per pixel. The key difference was a spectral configuration and the choice of a wavelength range used in the two studies. We used a blue optical setup covering a lot of prominent absorption lines in a wide wavelength range ($3900 < \lambda < 5300$ Å, same as used in the Monte-Carlo simulations presented earlier), while van Dokkum et al. (2016) used a narrow spectral region centered on Hα ($6444 < \lambda < 6679$ Å), which contains very few spectral lines. We applied Equation (2) to a stellar population template having age of 10 Gyr and [Fe/H] $= -1.5$ dex representative of a spectrum of DF 44 with all the parameters reported in the paper (σ, spectral resolution, sampling, etc.) and obtained an estimated σ uncertainty of 6.5 km s^{-1} fully consistent with 7 km s^{-1} presented by van Dokkum et al. (2016).

Similarly, we applied the formulae to the Binospec setup used by Chilingarian et al. (2019) using signal-to-noise ratios and stellar population parameters reported in the paper and obtained the uncertainty estimates for both v and σ fully consistent with the published values, which were taken directly from the minimization routine. Moreover, we tried both Equation (2) for average values of signal-to-noise and Equation (1) with the flux uncertainties provided by the

Binospec data reduction pipeline (Kansky et al. 2019). The results were generally consistent but the use of Equation (1) provided better agreement with the values from the minimization routine.

The derived expressions for uncertainties of kinematics quantify the amount of v and σ-sensitive information in an absorption-line spectrum, which can potentially be extracted from it. One can obtain this quantity empirically by computing derivatives $\partial\chi^2/\partial v$ and $\partial\chi^2/\partial\sigma$ from a template grid using finite differences. A similar approach was used by Chilingarian (2009), Chilingarian et al. (2011) to assess the quantity of age- and metallicity-sensitive information per wavelength bin. This information can be used to choose the optimal setup for a spectrograph to measure velocity dispersion or to choose the best spectral range for the data analysis. For example, Fabricant et al. (2013) empirically determined the optimal wavelength range to extract velocity dispersions from low-resolution galaxy spectra by running the full spectrum fitting code many times and adjusting the wavelength range. Using Equation (1) one can do it without running the code by simply analyzing template spectra.

There are several caveats of our approach if one plans to get quantitatively correct estimates of uncertainties as a quick alternative to Monte-Carlo simulations using Equation (1): (i) flux errors have to be correctly estimated and propagated through a data reduction pipeline that is used to produce spectra; (ii) strong template mismatch would affect the estimates of uncertainties, they will get underestimated; (iii) there is a degeneracy between σ and [Fe/H] (see Appendix A in Chilingarian et al. 2007b) when using stellar population models, which lead to increased σ uncertainties, e.g., their underestimation by Equation (1); (iv) there is a degeneracy between v and Gauss–Hermite $h3$ and as well between σ and $h4$, which would also lead to the underestimation of uncertainties by Equation (1) if one uses a 4th order LOSVD expansion in the analysis.

Despite all the caveats, the presented solution estimates v and σ uncertainties quickly and precisely and it can be used in a large range of situations from validating published kinematics of galaxies to preparing observational programs.

We thank D. Fabricant, I. Katkov, and A. Afanasiev for fruitful discussions and an anonymous referee for useful comments that improved the manuscript. I.C. is supported by the Telescope Data Center at Smithsonian Astrophysical Observatory. The authors acknowledge the Russian Science Foundation grant 19-12-00281 and the Program of development of M.V. Lomonosov Moscow State University for the Leading Scientific School "Physics of stars, relativistic objects and galaxies."

ORCID iDs

Igor V. Chilingarian, https://orcid.org/0000-0002-7924-3253
Kirill A. Grishin, https://orcid.org/0000-0003-3255-7340

References

Avni, Y. 1976, ApJ, 210, 642
Cappellari, M. 2008, MNRAS, 390, 71
Cappellari, M. 2017, MNRAS, 466, 798
Cappellari, M., & Emsellem, E. 2004, PASP, 116, 138
Chilingarian, I. 2006, PhD thesis, M.V. Lomonosov Moscow State Univ., Russia; Univeristé Claude Bernard Lyon, France. arXiv:astro-ph/0611893
Chilingarian, I., Prugniel, P., Sil'chenko, O., & Koleva, M. 2007a, in IAU Symp. 241, Stellar Populations as Building Blocks of Galaxies, ed. A. Vazdekis & R. R. Peletier (Cambridge: Cambridge Univ. Press), 175, arXiv:0709.3047
Chilingarian, I. V. 2009, MNRAS, 394, 1229
Chilingarian, I. V., Afanasiev, A. V., Grishin, K. A., Fabricant, D., & Moran, S. 2019, ApJ, 884, 79
Chilingarian, I. V., Mieske, S., Hilker, M., & Infante, L. 2011, MNRAS, 412, 1627
Chilingarian, I. V., Prugniel, P., Sil'Chenko, O. K., & Afanasiev, V. L. 2007b, MNRAS, 376, 1033
Chilingarian, I. V., Zolotukhin, I. Y., Katkov, I. Y., et al. 2017, ApJS, 228, 14
Fabricant, D., Chilingarian, I., Hwang, H. S., et al. 2013, PASP, 125, 1362
Fabricant, D., Fata, R., Epps, H., et al. 2019, PASP, 131, 075004
Kansky, J., Chilingarian, I., Fabricant, D., et al. 2019, PASP, 131, 075005
Le Borgne, D., Rocca-Volmerange, B., Prugniel, P., et al. 2004, A&A, 425, 881
Press, W. H., Teukolsky, S. A., Vetterling, W. T., & Flannery, B. P. 2007, Numerical Recipes 3rd Edition: The Art of Scientific Computing (3rd ed.; USA: Cambridge Univ. Press), doi:10.5555/1403886
Rix, H.-W., & White, S. D. M. 1992, MNRAS, 254, 389
van der Marel, R. P., & Franx, M. 1993, ApJ, 407, 525
van Dokkum, P., Abraham, R., Brodie, J., et al. 2016, ApJL, 828, L6
Westfall, K. B., Cappellari, M., Bershady, M. A., et al. 2019, AJ, 158, 231